JGR Oceans

RESEARCH ARTICLE
10.1029/2024JC021633

Key Points:

- Only powerful season-dependent Predictability Barrier can lead to large prediction errors for El Niño forecasts
- The initial errors of North (South) Pacific mainly affect the error evolution of central (eastern) Pacific
- The specific initial error modes identified by this study have more serious impacts on the final prediction of two types of El Niño events

Supporting Information:

Supporting Information may be found in the online version of this article.

Correspondence to:

S. Hu and W. Duan,
hushuju@lzu.edu.cn;
duanws@lasg.iap.ac.cn

Citation:

Zhang, J., Hu, S., Duan, W., Peng, J., & Hou, M. (2024). Consistent initial error modes causing the largest prediction errors and the strongest predictability barrier for two types of El Niño events in CMIP6. *Journal of Geophysical Research: Oceans*, *129*, e2024JC021633. https://doi.org/10.1029/2024JC021633

Received 24 JUL 2024
Accepted 27 NOV 2024

Author Contributions:

Conceptualization: Jingjing Zhang, Shujuan Hu, Wansuo Duan, Meiyi Hou
Data curation: Jingjing Zhang
Formal analysis: Jingjing Zhang, Jianjun Peng, Meiyi Hou
Funding acquisition: Shujuan Hu, Wansuo Duan
Investigation: Jingjing Zhang, Shujuan Hu, Wansuo Duan
Methodology: Jingjing Zhang, Wansuo Duan, Meiyi Hou
Project administration: Shujuan Hu, Wansuo Duan
Resources: Shujuan Hu, Wansuo Duan
Software: Jingjing Zhang, Jianjun Peng, Meiyi Hou
Supervision: Shujuan Hu, Wansuo Duan
Visualization: Jingjing Zhang
Writing – original draft: Jingjing Zhang
Writing – review & editing: Jingjing Zhang, Shujuan Hu, Wansuo Duan, Jianjun Peng

Consistent Initial Error Modes Causing the Largest Prediction Errors and the Strongest Predictability Barrier for Two Types of El Niño Events in CMIP6

Jingjing Zhang[1], Shujuan Hu[1], Wansuo Duan[2], Jianjun Peng[1], and Meiyi Hou[3]

[1]College of Atmospheric Sciences, Lanzhou University, Lanzhou, China, [2]Key Laboratory of Earth System Numerical Modeling and Application, Institute of Atmospheric Physics, Chinese Academy of Sciences, Beijing, China, [3]Department of Atmospheric Sciences, Yunnan University, Kunming, China

Abstract Based on the coupled conditional nonlinear optimal perturbation (C-CNOP) method, this study explores the season-dependent predictability barrier (PB) affecting the forecasts of two types of El Niño (central Pacific, CP; eastern Pacific, EP) events by using CMIP6 models. It is found that CP (EP) El Niño forecasts often occurs summer (spring) PB, and only powerful season-dependent PB can lead to large prediction errors. Further investigating the initial causes of the largest prediction errors and strongest PB, we find that the spatial pattern of initial errors consistently exhibits the sea temperature anomaly dipole of east positive–west negative in the equatorial Pacific, and errors over upper layers of North (South) Pacific are similar to the negative Victoria mode (South Pacific Meridional Mode). Physically, the mode evolution of initial errors in the equatorial Pacific, North and South Pacific are all positive feedback processes, which together ultimately lead to large cold biases over the central-eastern (CP) or eastern (EP) equatorial Pacific in December. Analysis shows that the initial error mode of North Pacific mainly affects the cold bias of the central Pacific, whereas the mode of South Pacific mostly controls the bias in the eastern Pacific. These initial error modes found in this study can have more serious impacts on forecasts of two types of El Niño events than that in previous studies. The results of this study offer valuable scientific guidance for the adaptive observation of ENSO, which will likely be able to maximize the prediction skills for two types of El Niño events.

Plain Language Summary El Niño-Southern Oscillation (ENSO) is the most significant interannual signal causing global climate anomalies; thus, its accurate forecast has attracted much attention. The central Pacific (CP) and eastern Pacific (EP) El Niño forecasts are closely associated with the season-dependent predictability barrier (PB), which refers to the sharp drop of CP (EP) El Niño prediction skills across the boreal summer (spring) season. Our study found that only powerful season-dependent PB can lead to large prediction errors. Furthermore, for such forecasts with the largest prediction errors and strongest PB, the corresponding initial errors have consistent spatial pattern and evolutionary feature. Physically, the evolutions of such initial errors found in this study in the equatorial Pacific, North and South Pacific are all to cause larger cold biases over the equatorial Pacific at the final time. Therefore, if we deploy observations by using the adaptive observation in some critical areas of the equatorial Pacific, North and South Pacific, where the initial errors are large and concentrated, it will be possible to maximize prediction skills for two types of El Niño events.

1. Introduction

The El Niño-Southern Oscillation (ENSO), which is the dominant mode on the interannual variability of the large-scale coupled ocean-atmosphere, originates in the tropical Pacific but influences weather and climate globally (Bjerknes, 1969; Latif et al., 1998; Mcphaden et al., 2006; Zhang et al., 2016). Sometimes, ENSO has tremendous global climate impacts and even causes severe disasters. For instance, widespread climate anomalies, including droughts and floods, have occurred globally, resulting in serious injuries and property damages after the peak of the three strongest El Niño events in 1982/1983, 1997/1998, and 2014/2016 (FAO, 2016; McPhaden, 1999; McPhaden et al., 2006; Philander, 1983; Sánchez-Murillo et al., 2017; Valle et al., 1987; Zhai et al., 2016). Accordingly, it is crucial to provide skillful ENSO forecasts.

With the progress in theoretical studies, the development in coupled models and the improvement in initialization schemes, the skills of real-time forecasts for ENSO have improved considerably over the past four decades (Tang

et al., 2018). Currently, more than 20 forecast models can provide effective predictions of ENSO warm and cold events 6–12 months ahead (Barnston et al., 2012; Zheng & Yu, 2017). However, ENSO forecasts have not improved steadily and still present large uncertainties; in particular, ENSO prediction skills have declined rather than increased since 2000, even with the ongoing improvement of forecast models (Barnston et al., 2012; Hou et al., 2022).

One major possible reason for the shift in the ENSO prediction skills is ENSO diversity (Ren et al., 2018; Zheng & Yu, 2017). Traditionally, the action center of the sea surface temperature (SST) anomalies of ENSO is usually located in the eastern Pacific cold tongue (Kug et al., 2009; Timmermann et al., 2018). However, many studies have revealed that a different type of El Niño—as compared to the traditional eastern Pacific (EP) El Niño—began to appear frequently since the late 1990s (Ren & Jin, 2011; Wang & Ren, 2017). This trend has sparked a new wave of ENSO research. For this type of El Niño, the action center of SST anomalies appears in the central Pacific, so we will refer it as the central Pacific (CP) El Niño (Zheng et al., 2014; Zheng & Yu, 2017). The differences between EP and CP El Niño are bound to have different impacts on weather and climate (Chen et al., 2019; Zhang et al., 2016). However, the limited understanding of dynamic mechanisms for CP El Niño hinders the accurate simulation of El Niño types and intensities in models (Hou et al., 2019; Qi et al., 2021). Moreover, CP El Niño will likely become more frequent under global warming, increasing the uncertainty of ENSO forecasts (Yeh et al., 2009, 2014). Therefore, it is necessary to clarify the differences in predictability dynamics between two types of El Niño events for improving the predictive power of ENSO.

Another important issue that contributes to the uncertainty of ENSO forecasts is the spring predictability barrier (SPB), which is a long-standing problem. Webster and Yang (1992) described the SPB as a rapid decline of observation-prediction correlations of SST in the boreal spring. From the perspective of error growth, the SPB refers to the phenomenon that ENSO forecasting exhibits significant error growth during the boreal spring when predictions are made prior to spring (Duan et al., 2009; Duan & Wei, 2013; Mu et al., 2007; Yu et al., 2009). There are various hypotheses about the occurrence of the SPB phenomenon. Some studies argue that the SPB is the result of the annual cycle of the background condition in the tropical Pacific (Jin et al., 2019; Lau & Yang, 1996; Levine & McPhaden, 2015; Liu et al., 2019; Thompson & Battisti, 2001; Torrence & Webster, 1998; Webster, 1995). Because the signal-to-noise ratio of SST tends to be lowest in spring, which destroys the persistence of ENSO in this season (Samelson & Tziperman, 2001; Xue et al., 1994). Meanwhile, others emphasized the role of initial errors in the SPB. A number of studies have demonstrated that the decline of ENSO prediction skill in spring stems more from initial errors than from unpredictable noise, and thus, the prediction skill across spring can be significantly enhanced by improving initialization (Chen et al., 1995, 2004; Lee et al., 2018; McPhaden, 2003). Going further, Mu et al. (2007) demonstrated that a 'significant SPB' might be the result of the combined effect of three factors: the climatological annual cycle, the El Niño event itself, and the initial error pattern. The first two factors are robust in existence, while the third factor is artificially induced. Even if the annual cycle is robust in predictive models, specific initial error patterns are required to generate the SPB for an El Niño event (Duan & Wei, 2013).

The study about the initial errors belongs to the first type of predictability problems proposed by Lorenz (1975) (see a review by Mu et al., 2017). The perfect model predictability experiments assume that the numerical model is perfect, and it only focuses on the impact of initial errors on prediction uncertainty. Thus, many studies usually rely on the perfect model predictability experiments to explore the above SPB-related initial errors (Duan et al., 2009; Duan & Hu, 2016; Hou et al., 2019; Qi et al., 2021; Yu et al., 2009; Zhang et al., 2015). Some early studies conducted the perfect model predictability experiments using the intermediate-complexity Zebiak-Cane (ZC) model to explore the initial errors leading to significant SPB for EP El Niño events (Duan et al., 2009; Yu et al., 2009). However, the limitation of the ZC model is that it only considers interannual variability in the tropical Pacific. Therefore, researchers further explored the SPB-related initial errors using CMIP5 coupled models (Zhang et al., 2015) and the Community Earth System Model (CESM) (Duan & Hu, 2016) for EP El Niño.

Furthermore, the frequent occurrences of CP El Niño have prompted more studies to focus on the predictability dynamics for CP El Niño and the differences between two types of El Niño events, aiming to improve the ENSO prediction capability. Tian and Duan (2016) demonstrated that the prediction of CP El Niño also exhibits the SPB phenomenon in the ZC model. Recently, Hou et al. (2019) found that summer predictability barrier (PB) is

commonly occurring for CP El Niño. Simultaneously, more and more studies have emphasized the important role of the subtropical Pacific in the occurrence and prediction for two types of El Niño (Ding et al., 2015; Hong et al., 2014; Hou et al., 2019; Min et al., 2017; Qi et al., 2021; Vimont et al., 2003; Wang et al., 2019; Yeh et al., 2015; Yu & Kim, 2011; Zhang et al., 2014). From these previous studies, EP El Niño events seem to be closely linked to the South Pacific, whereas the Northern Pacific climate modes play a more prominent role in influencing CP El Niño. For example, Hou et al. (2019) used a predictability data analysis approach to investigate the effect of initial SST accuracy in different Pacific regions on the prediction of two types of El Niño events in the CMIP5 coupled model. However, Hou et al. (2019) only considered the forecasts that occur season-dependent PB and have larger prediction errors, and the initial errors causing such forecasts are the SPB-related initial errors commonly analyzed in the previous studies. More specifically, they did not investigate the initial errors with the greatest impact on the prediction results, and the initial errors obtained from such extreme-value problem are not necessarily the above SPB-related initial errors.

Undoubtedly, it is most desirable to reduce such initial errors that have the greatest impact on the prediction results during initializing the model; finally the prediction skills are likely to be the highest. Because although the season-dependent PB and the prediction error are closely related, the relationship between the two is nonlinear. Therefore, when we examine the forecast series with the greatest impact on the prediction results, that is, those with the maximum prediction errors, it is natural to be very concerned about whether the phenomenon of powerful season-dependent PB occurs in those forecast series? As previously mentioned, the generation of season-dependent PB requires specific initial error patterns. So if those forecast series with the largest prediction errors experience season-dependent PB, what are the spatial structures and evolutionary characteristics of the related initial errors? And how does the uncertainty in the tropical and subtropical Pacific contribute to the development of these initial errors? To avoid the limitation that results are model-dependent, we select the more coupled models with better performance in latest CMIP6 and comprehensively investigate the initial errors with largest prediction errors, expecting to answer the above questions. In addition, we compare the similarities and differences between the initial errors with largest prediction errors and the SPB-related initial errors. Eventually, if we can find some specific initial errors, it will be possible to significantly minimize the prediction errors in the actual forecasts.

The remainder of this paper is organized as follows. Section 2 describes the data and the method used in this study. Section 3 explores the predictability barrier and prediction errors in different forecast series for CP and EP El Niño events. Section 4 focuses on the initial errors with largest prediction errors and their seasonal growth mechanisms for the two types of El Niño. In Section 5, we discuss the differences between the above initial errors and the SPB-related initial errors. Lastly, Section 6 provides a summary and discussion.

2. Data and Method

2.1. CMIP6 Model Data

CMIP6 is the program with the largest number of models, the most complete scientific experiments, and the largest amount of simulation data, since the implementation of Coupled Model Intercomparison Project (CMIP). Further information about the CMIP6 protocol can be found by Eyring et al. (2016). Compared to the CMIP5 models, CMIP6 models tend to perform better in terms of the background climatology, pattern, and diversity of ENSO (Planton et al., 2021). Therefore, we use offline CMIP6 data to investigate the spatial structures and evolutionary characteristics of initial errors that lead to the largest prediction errors for two types of El Niño events in this study. In fact, the CMIP6 models have different abilities to simulate the two types of El Niño events, and in particular, the simulation of CP El Niño is still poor (Hou & Tang, 2022). Referring to the assessments of Bellenger et al. (2014) and Hou and Tang (2022), we evaluate the preindustrial Control (pi-Control) runs of 37 CMIP6 climate model integrations in terms of both the background climate and the El Niño events (Figure S1–S8 and Table S1–S2 in Supporting Information S1). We finally choose 6 models, which can reasonably simulate the CP and EP El Niño events. Specific model configurations and affiliations are listed in Table 1. Sea surface temperature (SST), zonal and meridional wind components, and ocean subsurface temperature (at depths of 5–155 m) are obtained from the outputs of the 6 coupled models. All variable fields are uniformly interpolated into the $1° \times 1°$ grids using the Climate Data Operators (CDO) tools (Schulzweida, 2022), and the time is chosen as the first 499 years of integration in each model. All outputs are monthly mean data.

Table 1
Basic Information of Six CMIP6 Coupled Models

Model	Institute/country	Resolution (lon × lat, vertical)	
		Atmosphere	Ocean
CAMS-CSM1-0	CAMS/China	320 × 160, L31	360 × 200, L50
CMCC-CM2-SR5	CMCC/Italy	288 × 192, L30	362 × 292, L50
FGOALS-f3-L	CAS/China	360 × 180, L32	360 × 218, L30
HadGEM3-GC31-LL	MOHC/UK	192 × 144, L85	360 × 330, L75
MIROC6	MIROC Consortium/Japan	256 × 128, L81	360 × 256, L63
MRI-ESM2-0	MRI/Japan	320 × 160, L80	360 × 364, L61

2.2. The Couple Conditional Nonlinear Optimal Perturbations Method

As mentioned above, the pi-Control experiments are adopted in the present study. The pi-Control experiments are driven under a constant external forcing (fixing greenhouse gases, aerosols, ozone, and solar constant at 1850) and are the reference for other runs such as historical, climate sensitivity, and so on. Based on pi-Control outputs of CMIP6 coupled models, the couple conditional nonlinear optimal perturbations (C-CNOP) method proposed by Duan et al. (2024) can help us to explore the predictability dynamics of two types of El Niño events in terms of initial errors growth. This method is expected to adequately capture the nonlinear unstable growth of initial uncertainties, while also taking into account the effect of the coupling processes uncertainty on initial perturbations. Below we give a brief introduction to the C-CNOP method; more detailed descriptions are provided in Duan et al. (2024).

First, we abstract the multisphere coupled dynamical system as a conceptual model that includes the interaction of fast variables (such as weather variability in the atmosphere) and slow variables (such as sea temperature evolution). In this study, we analyze forecasts for the slow variable X (e.g., SST); the governing equations for X are expressed as follows:

$$\begin{cases} dX = F(X,Y,t)\,dt + f_X dt \\ X|_{t=0} = X_0 \end{cases}, \quad \Omega \times [0,T] \tag{1}$$

where F is a nonlinear functionality, Y is a fast variable, t is time, T is forecast time, $t \in [0,T]$, X_0 is the initial state, f_X represents the external forcing of the slow variable X and is a constant in the pi-Control runs.

Then, by integrating Equation 1 from t_a to t_b ($t_a < t_b < T$), the corresponding state X_{t_b} at the future time t_b can be derived as follows:

$$X_{t_b} = X_{t_a} + \int_{t_a}^{t_b} F(X,Y,t)\,dt + f_X(t_b - t_a) \tag{2}$$

We pick two time periods $[t_{01},t_1]$ and $[t_{02},t_2]$ from the time series of coupled model data with initial states denoted as $X_{t_{01}}$ and $X_{t_{02}}$, respectively. According to Equation 2, if the two time periods have same length, then, the difference between two final states X_{t_1} and X_{t_2} can be described as follows:

$$X_{t_2} - X_{t_1} = X_{t_{02}} - X_{t_{01}} + \int_{\sum} [F_{t_{02}} - F_{t_{01}}]\,dt \tag{3}$$

where $F_{t_{02}}$ and $F_{t_{01}}$ are the F in two integrations of Equation 2 over the time intervals $[t_{01},t_1]$ and $[t_{02},t_2]$, respectively. And $\sum$ is the time interval $[t_{01},t_1]$ or $[t_{02},t_2]$. From Equation 3, it is known that the difference between X_{t_1} and X_{t_2} can be considered to be derived by the model Equation 2 that are only caused by initial difference $X_{t_{02}} - X_{t_{01}}$. Because it does not involve model errors, the functional form of F is not changed. Further, if the series during the time period $[t_{01},t_1]$ is regarded as an "observation", the series during $[t_{02},t_2]$ can be

referred as "prediction" of "observation". Therefore, "prediction error" at the termination time is only caused by "initial error" implied by $X_{t_{02}} - X_{t_{01}}$.

For a given time series, we can build different optimization problems to analyze different initial errors if we consider different constraints. For example, if we consider the initial errors that can lead to the largest prediction errors, the optimization problem is established as follows:

$$J(x_{m,n}) = MAX(\|X_{T_{m,n}} - X_{T_m}\| / \|X_{0_{m,n}} - X_{0_m}\|), \quad 1 \le n < N;\ m = 1, 2, ..., M \tag{4}$$

where $x_{m,n}$ represents the initial errors that can lead to the largest prediction errors at the forecast time T, based on the m–th "observation" and its n "predictions". $n < N$ represents the number of forecast series, which can be broadly selected from the model outputs. M represents the number of observations. Therefore, Equation 4 provides the initial error that is statistically optimal and that contains the impact of interaction uncertainties between fast and slow variables.

In this study, we select 10 typical CP El Niño events and 10 typical EP El Niño events as one-year "observations" from the 499-year integrations of each model. The typical El Niño events refer to warming in early boreal spring and peaking at the end of the year. For each of one-year "observations", we select the remaining 497 one-year periods (the last year is also ignored) of all 499-year integrations as "predictions" (12 months lead time) for an "observation". This will yield 4970 "predictions" for 10 CP and 10 EP El Niño events of each model, respectively. Then, the corresponding prediction errors $E(t)$ are only caused by the initial errors. The calculation formula is as follows:

$$E(t) = \|X^p(t) - X^o(t)\| = \sqrt{\frac{\sum_{i,j}[X^p_{i,j}(t) - X^o_{i,j}(t)]^2}{S}} \tag{5}$$

where X^p represents "prediction", X^o is "observation", (i,j) indicates grid points in the Niño4 area [5°S−5°N, 160°E−150°W] for CP El Niño (the Niño3 area [5°S−5°N, 150°W−90°W] for EP El Niño), and S is the total number of grid points.

Next, we measure the seasonal growth of prediction errors. Mu et al. (2007) proposed that the tendency of prediction error can be described as the slope k of curve $E(t)$, which can be approximated as follows for the monthly data used in the present study:

$$k = \frac{\partial E(t)}{\partial t} \approx \frac{E(t_2) - E(t_1)}{t_2 - t_1} \tag{6}$$

with the interval of $t_2 - t_1$ being 1 month ($t_2 > t_1$). The growth rate of prediction errors during one season can be calculated with the average of the three successive monthly slopes k in this season (i.e., a 3-month running mean was applied for k, denoted as $k^{season}_{t'}, t' \in [1, T-1]$). Then, if the growth rate of prediction errors for a particular season is the largest in most forecasts, the season-dependent PB is deemed to occur. The larger the positive seasonal growth rate, the stronger the season-dependent PB.

3. Predictability Barrier and Prediction Errors

We first explore the PB and prediction errors for two types of El Niño events by using the C-CNOP method described in Section 2.2. As mentioned previously, the so-called season-dependent PB in ENSO forecasts refers to the significant growth of prediction errors in a particular season. Figure 1 shows the number of predictions (CP El Niño) and the main months (CP and EP) with the maximum growth rates of prediction errors. It is shown that in most models, the prediction errors of CP El Niño events mainly increase significantly during July–September (Figures 1a–1g). For EP El Niño events, the prediction errors mostly grow significantly from April to June (Figure 1h). Therefore, consistent with previous studies (Hou et al., 2019; Tao et al., 2023), the CP El Niño forecasts tend to experience the summer PB, while the EP El Niño forecasts often occur the spring PB. Moreover, the positive error growth rates of EP El Niño are generally larger than that for CP El Niño, indicating the stronger season-dependent PB for EP El Niño events (see Figure S9 in Supporting Information S1).

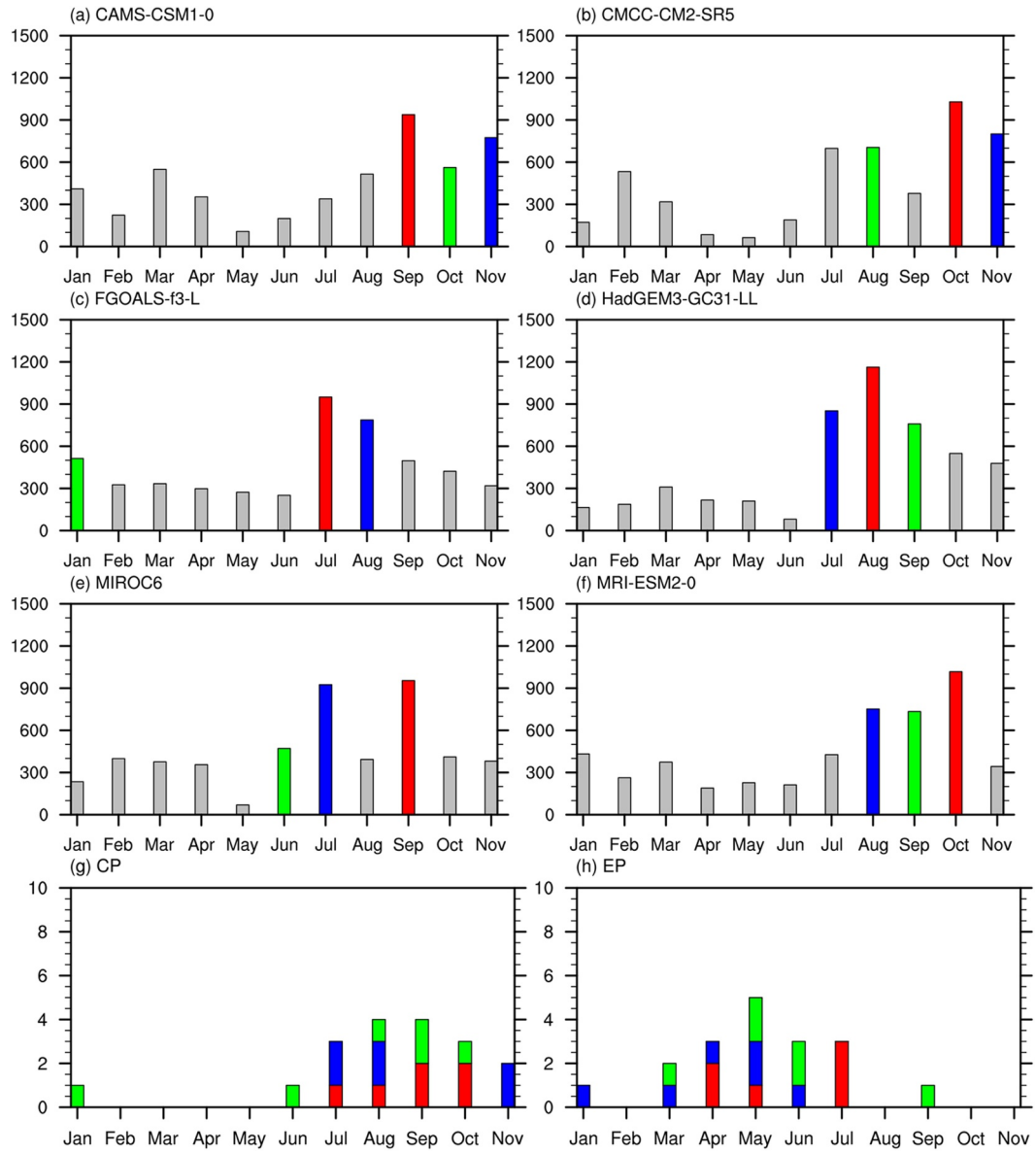

Figure 1. (a)–(f) shows the number of predictions with the maximum growth rates of prediction errors by month in each model for CP El Niño (4970 predictions in total). The red bar shows the first largest number of predictions, and the blue (green) bar corresponds to the second (third) largest number of predictions. (g) and (h) show the number of models with the first (red), second (blue), and third (green) largest number of predictions by month for CP and EP El Niño, respectively.

However, not all forecasts experience spring PB (EP El Niño) or summer PB (CP El Niño). Even when the season-dependent PB occurs in some forecasts, the resulting prediction errors are not always large (pink regions in Figure S10 in Supporting Information S1). Next, we only focus on the series with large prediction errors, and then establish three different types of optimization problems based on different constraints for comparative analysis (see Table 2). According to the method in Section 2.2, we give the corresponding mathematical expression in Table 2. First, the main emphasis in this study is on the series with the greatest impact on forecasts, namely those with the largest prediction errors. Based on Section 2, the first 5 series with the largest prediction errors are selected from the 497 "predictions" of each "observation"; consequently, each model generates 50 "predictions" for selected 10 CP or 10 EP El Niño (for convenience, denoted as "Max Pred"). Similarly, we also select the first 5 series with the largest seasonal error growth rate (i.e., with the strongest PB; denoted as "Max PB"). Third, we randomly choose 50 series from the "predictions" that experience the spring PB (EP El Niño) or summer PB (CP El Niño) and have large prediction errors at the final time (referred to as "Often PB"). Consequently, "Often PB"

Table 2
Prediction Series of Different Groups of Optimization Problems

	Description	Mathematical expression
Max Pred	For m–th observation, choose the first 5 prediction series $X1_{t_{m,n}}$ with the largest prediction errors	$t \in [0,T], \quad n \in Index1_m^5$ $Index1_m^5 = Arg\max_n{}^5(E_{T_{m,n}}), \quad 1 \le n < N$
Max PB	For m–th observation, choose the first 5 prediction series $X2_{t_{m,n}}$ with the largest seasonal error growth rate	$t \in [0,T], \quad n \in Index2_m^5$ $Index2_m^5 = Arg\max_n{}^5(kmax_{m,n}), \quad 1 \le n < N$ $kmax_{m,n} = Max(k_{t}^{season}{}_{m,n}), \quad t' \in [1, T-1]$
Often PB	For m–th observation, randomly choose 50 prediction series $X3_{t_{m,n}}$ that experience the spring PB (EP El Niño) or summer PB (CP El Niño) and have large prediction errors	$t \in [0,T], \quad n \in Index3_m^{50}$ $Index3_m^{50} = Random_n^{50}\left(SPB_{m,n} \cap E_{m,n}^{l\ \arg\ e}\right), 1 \le n < N$ $\left\{E_{m,n}^{l\ \arg\ e} \middle\| E_{T_{m,n}} > Average_t(E_{t_{m,n}})\right\}$
Often PB II	As above, but randomly choose 5 prediction series $X4_{t_{m,n}}$	$t \in [0,T], \quad n \in Index4_m^5$ $Index4_m^5 = Random_n^5\left(SPB_{m,n} \cap E_{m,n}^{l\ \arg\ e}\right), 1 \le n < N$ $\left\{E_{m,n}^{l\ \arg\ e} \middle\| E_{T_{m,n}} > Average_t(E_{t_{m,n}})\right\}$

of each model generates 500 predictions for the selected 10 CP or 10 EP El Niño. "Often PB" is the series commonly analyzed in previous studies, and represents predictions in which PB universally occurs. The first meaning of "Often" refers to the fact that CP El Niño forecasts universally experience summer PB and EP El Niño forecasts commonly occur spring PB. The second meaning of "Often" is reflected in the number of forecasts, that is, the filtered forecasts are often more than those under the first two constraints. Therefore, it is not known whether the seasonal-dependent PB will occur in "Max Pred" and "Max PB". If it does, what are the similarities and differences between the both and "often PB"?

Mathematically, the *Arg* max function is used to find the parameter value that makes the function maximum. In this study, $Arg\max_n{}^5$ represents the parameter n values for which the first 5 maximum values are found. $Random_n^{50}$ represents the parameter n values for which 50 values are randomly selected.

To compare the PB intensity of the three types of prediction series under same conditions, we again randomly select 5 series from the "predictions" that experience the seasonal-dependent PB and have large prediction errors at the final time (denoted as "Often PB II", also shown in Table 2). Figure 2 shows the error growth rates of "Max Pred", "Max PB", and "Often PB II" for CP El Niño events (see Figure S11 in Supporting Information S1 for EP El Niño). It is clear that "Max Pred" and "Max PB" for CP El Niño generally present the summer PB (June–August), similar to "Often PB II" (July–September), only slightly a month ahead. Likewise, EP El Niño events tend to experience the spring PB (April–June) for three types of prediction series. However, the seasonal-dependent PB of "Max Pred" and "Max PB" for two types of El Niño events are stronger than that of "Often PB II". The evolutionary behaviors of prediction errors of "Max Pred", "Max PB", and "Often PB" for CP and EP El Niño are shown in Figure 3 and Figure S12 in Supporting Information S1. For "Often PB", most of predictions exhibit significant error growth in the boreal summer (CP El Niño) or spring (EP El Niño), and have large prediction errors at the final time. However, there are some predictions that have significant seasonal-dependent PB, but the prediction errors at the final time are relatively smaller, and vice versa. As mentioned in the introduction, specific initial errors are the necessary condition to generate the seasonal-dependent PB for two types of El Niño events. It means that if the seasonal-dependent PB is weakened by reducing the specific initial errors, the prediction error does not necessarily decrease (see Figure S13a in Supporting Information S1). Also, reducing the

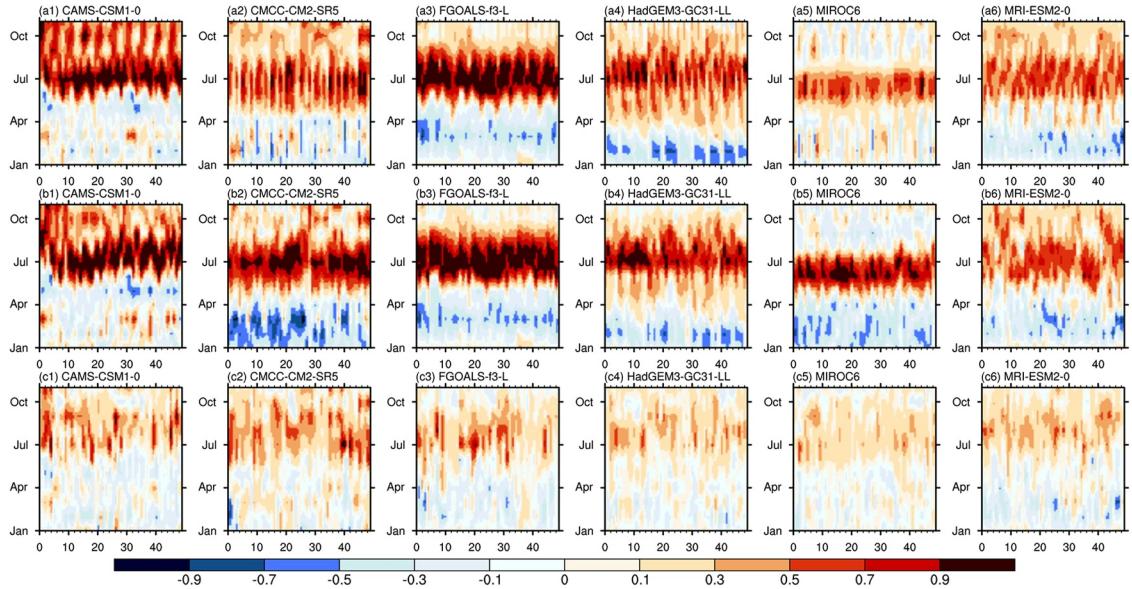

Figure 2. Monthly growth rates of prediction errors for the three types of prediction series (50 predictions on the horizontal axis) in each model. (a), (b), and (c) denote the "Max Pred", "Max PB", and "Often PB II" for CP El Niño events, respectively. Positive values (red color) indicate increases of prediction errors, and negative values (blue lines) indicate decreases of prediction errors.

prediction error may not always weaken the seasonal-dependent PB (Figure S13b in Supporting Information S1), which breaks our habitual thinking. In contrast, "Max Pred" and "Max PB" exhibit significant seasonal-dependent PB in almost all series, and prediction errors are overall larger at the final time. Upon further comparison, the error evolutions of "Max Pred" are very similar to that of "Max PB"; thus, the intensity of seasonal-dependent PB and the magnitude of prediction errors are also very similar. The above results indicate that only powerful season-dependent PB can lead to large prediction errors. Therefore, we infer that the initial errors of "Max Pred" and "Max PB" may be different from that of "Often PB", whereas the initial errors of "Max Pred" may be very similar to that of "Max PB". Then, which characteristics of initial errors for the three types of prediction series are more likely to cause the seasonal-dependent PB? Moreover, how do initial errors evolve and impact the forecasts for two types of El Niño events?

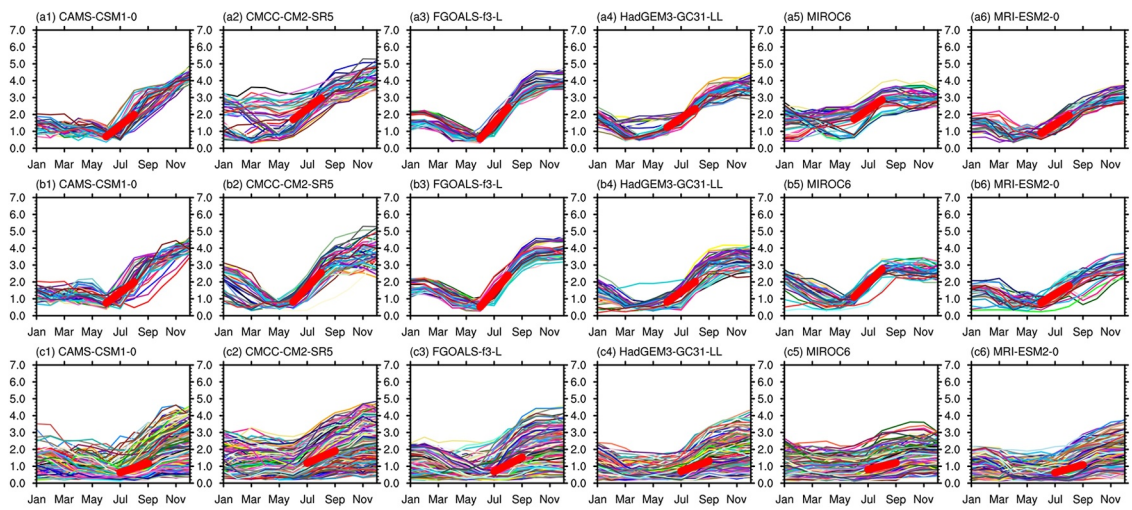

Figure 3. The evolution of prediction errors for three types of prediction series in each model. (a), (b), and (c) denote the "Max Pred", "Max PB", and "Often PB" for CP El Niño events, respectively. The prediction errors tend to present the significant growth (i.e., the large slope indicated by the short thick red line) in the period June–August ("Max Pred" and "Max PB") or July–September ("Often PB"). All composite trends (short thick red line) in six models are significant at the 99% confidence level.

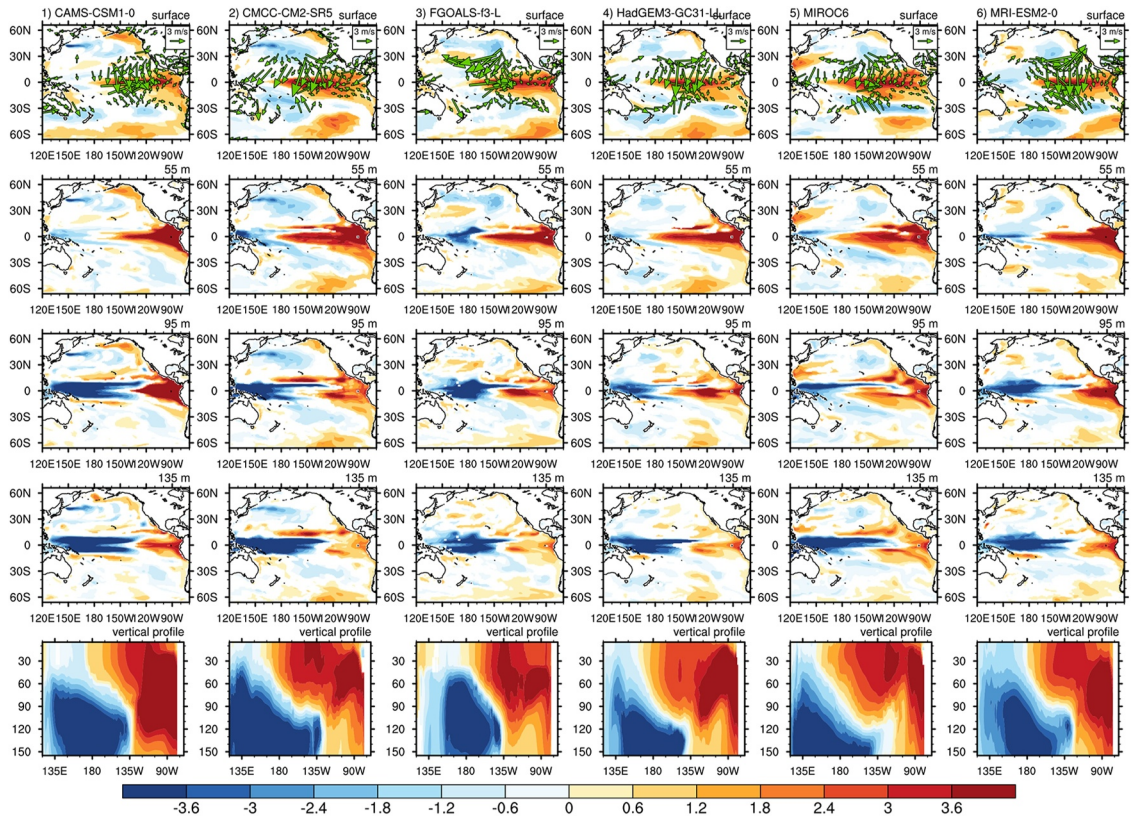

Figure 4. Composite of anomalous ocean temperature (shaded) (units: °C) and surface wind (vectors) (units: m/s) components of CP-Type-1 initial errors for "Max Pred". The top 4 rows correspond to different ocean levels, from the sea surface to 55 m and then to 95 m and 135 m. The last row shows the meridional average of ocean temperature anomaly over 5°S–5°N. The composite of initial SST errors that reach 90% significance level is colored. Showing significant surface wind vectors at the 90% level.

4. The Initial Errors That Cause the Largest Prediction Errors and Their Related Evolutions

To address the questions proposed in Section 3, the empirical orthogonal function (EOF) analysis is used in the above initial SST errors in Pacific regions [66.5°S−66.5°N, 120°E−70°W] for "Max Pred", "Max PB", and "Often PB". For each prediction series, we select initial errors that are highly related to the first three EOF modes. Specifically, if a principal component (PC) value is greater than the average of all positive PCs for each EOF mode, the corresponding initial SST error is deemed highly positively related to that EOF mode. Conversely, if a PC value is less than the average of all negative PCs, the corresponding initial SST error is considered to be highly negatively related to the EOF mode. Further, we composite the corresponding initial errors that are highly positively or negatively related to each EOF mode, resulting in six patterns of composite initial errors. The above steps are repeated for each of predetermined models. It is found that there are two types of composite initial SST errors with relatively consistent patterns in all six models. For convenience, we denote the two types of composite initial errors as CP-Type-1 and CP-Type-2 errors for CP El Niño (EP-Type-1 and EP-Type-2 errors for EP El Niño), respectively. In this section, we concentrate on the spatial structures and evolutionary characteristics of the two types of composite initial errors for "Max Pred".

Figure 4 shows the spatial patterns of CP-Type-1 initial sea temperature errors at different depths for "Max Pred". The results show that CP-Type-1 errors exhibit the SSTA dipole structure of east positive–west negative in the equatorial Pacific for all the selected models, that is, warm anomalies in the upper layers (above 90 m) of the eastern equatorial Pacific and cold anomalies in the subsurface (90–155 m) of western equatorial Pacific. In addition, for most of the models, the CP-Type-1 errors over the upper layers of North Pacific are similar to the negative Victoria mode (VM) described by Ding et al. (2015), and the negative anomalies mainly in the upper layers of South Pacific are generally similar to the negative South Pacific Meridional Mode (SPMM) (see Min

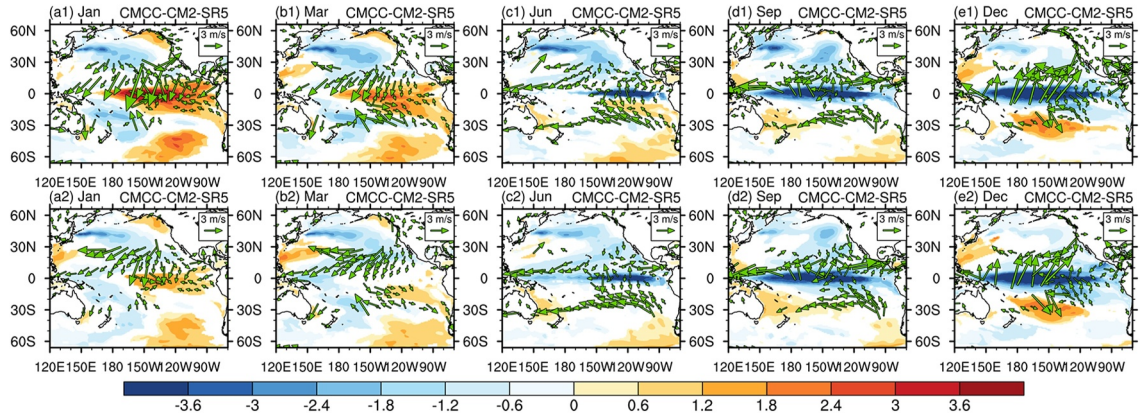

Figure 5. Composite evolutions of anomalous ocean temperature (shaded) (units: °C) and surface wind (vectors) (units: m/s) of the two types of errors for "Max Pred", as shown in January, March, June, September, and December from left to right. (1) and (2) denote the CP-Type-1 and CP-Type-2, respectively. The shaded areas denote those exceeding the 90% significance level. Only surface wind vectors significant at the 90% level are shown. This figure shows the results of the CMCC-CM2-SR5 model.

et al., 2017). CP-Type-2 errors are very similar to CP-Type-1 in the equatorial Pacific, North and South Pacific, showing good pattern consistency (Figure S14 in Supporting Information S1). Differently, the magnitude of CP-Type-2 errors is overall smaller than that of CP-Type-1. In summary, both CP-Type-1 and CP-Type-2 errors indicate that the forecasts of CP El Niño events are sensitive to initial errors not only in tropical Pacific but also in North and South Pacific. Then, how do these two types of initial errors for "Max Pred" evolve and affect the forecasts of CP El Niño?

All six models exhibit resemble dynamical behaviors. To clearly show the evolution of errors, we take the CMCC-CM2-SR5 model as an example (Figure 5; all models see Figure S15 and S16 in Supporting Information S1). It is shown that the CP-Type-1 and CP-Type-2 errors start with the decay of El Niño-like mode, and then transition to the development of La Niña-like mode. The transition occurs around June. The two types of initial errors eventually triggered cold biases of prediction in the central-eastern equatorial Pacific, especially in the Niño4 area. Physically, the warm SSTA over the eastern equatorial Pacific in CP-Type-1 and CP-Type-2 boosts strong westward winds in the central equatorial Pacific, which evokes the upwelling eastward-propagating Kelvin waves in the ocean. Corresponding Kelvin waves gradually transmit the cold SSTA in the lower of western equatorial Pacific to be eastward and upward. Once the cold SST errors in the central-eastern equatorial Pacific begin to occur, eastward wind anomalies will be generated, and thereafter, the cold anomalies gradually develop under the Bjerknes positive feedback mechanism (Bjerknes, 1969). Following the mechanism of wind–evaporation-SST feedback (WES; Xie & Philander, 1994), the negative SPMM-like cold SSTAs over the South Pacific could sustain themselves and penetrate into the equatorial Pacific, which accelerates the disappearance of warm SSTA (Zhang et al., 2014). The induced southeasterly wind anomalies also play an important role in reversing the former westerly winds in the central equatorial Pacific, which contributes to the development of cold SSTA in the central-eastern equatorial Pacific at the following time (Min et al., 2015). Similarly, the negative VM-like cold SSTAs over the North Pacific are able to penetrate into the equatorial Pacific via WES feedback, and the induced wind anomalies are dispersed in the central equatorial Pacific, which contributes to the earlier emergence and development of cold SSTA over the central-eastern equatorial Pacific (Ding et al., 2015; Su et al., 2014). The contributing processes in the equatorial Pacific, North and South Pacific ultimately combine to result in large negative errors over the central-eastern equatorial Pacific in December.

Figure 6 shows the composite initial errors of EP-Type-1 for "Max Pred". It can be seen that the spatial patterns of EP-Type-1 and EP-Type-2 (not shown) are generally similar to that of CP-Type-1 and CP-Type-2, respectively. That is, the equatorial Pacific exhibits the SSTA dipole structure of east positive–west negative, the upper layers of North Pacific are similar to the negative VM mode, and the upper layers of South Pacific show a general resemblance to the negative SPMM mode. Similarly, the mode difference between EP-Type-1 and EP-Type-2 is similar to that of CP-Type-1 and CP-Type-2, that is, mainly in the magnitude. However, the difference is that the EP-Type initial errors in most models tend to have weaker warm SSTA in the central-eastern equatorial Pacific (Figure S17 in Supporting Information S1). Also, the EP-Type-1 and EP-Type-2 initial errors show the

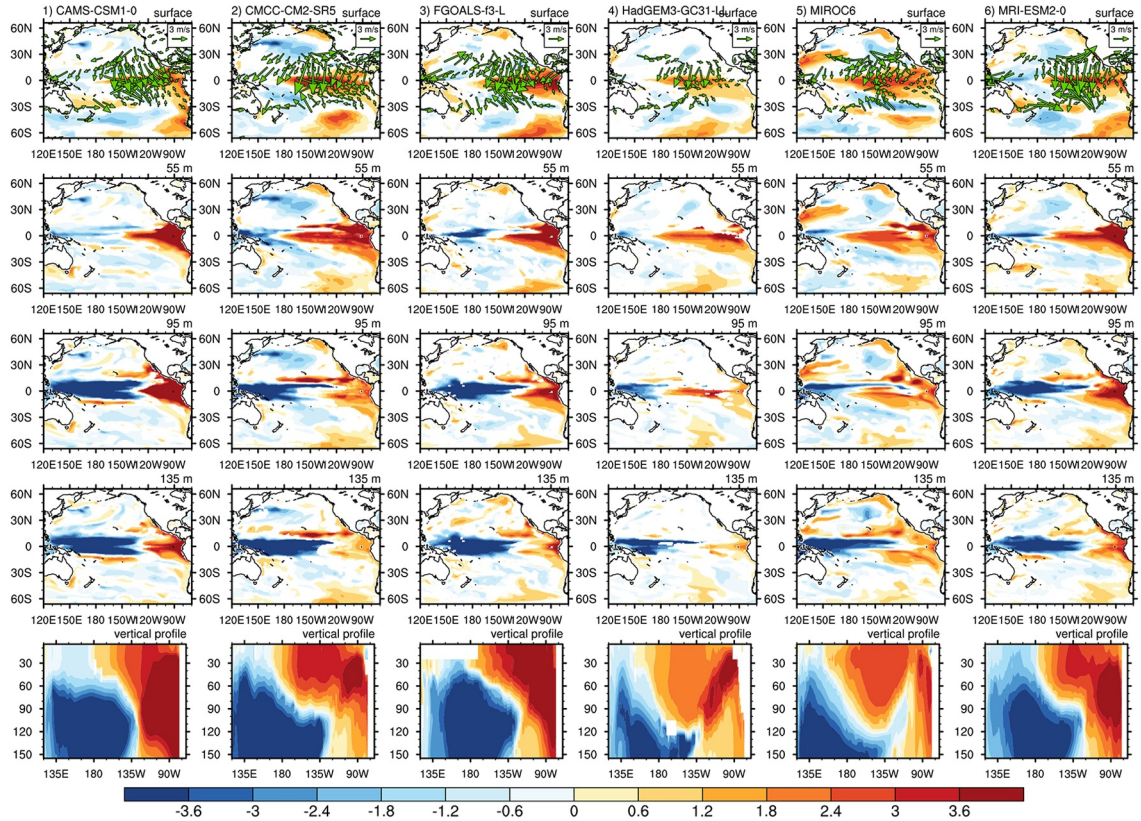

Figure 6. As in Figure 4, but for the EP-Type-1 initial errors for "Max Pred".

evolutionary feature from the El Niño-like decay to the La Niña-like development (Figure S18 in Supporting Information S1). But unlike CP-Type errors, the transition of the EP-Type pattern (from warm SSTA to cold SSTA in the equatorial Pacific) occurs in around April–May, and ultimately triggers more easterly regions of the equatorial cold bias in December (Figure 7). Further, by comparing the errors evolution between two types of El Niño events, we found that the SSTA mode of negative VM-like for CP El Niño plays a stronger role than that for EP El Niño, whereas the negative SPMM-like SSTA mode of EP El Niño plays a stronger role than that of CP El Niño. It is consistent with the previous studies in which the North Pacific process mainly favors the development of SSTA in the central equatorial Pacific, whereas the South Pacific process mainly favors the development of SSTA in the eastern equatorial Pacific (Hou et al., 2019; Min et al., 2017; Zhang et al., 2014).

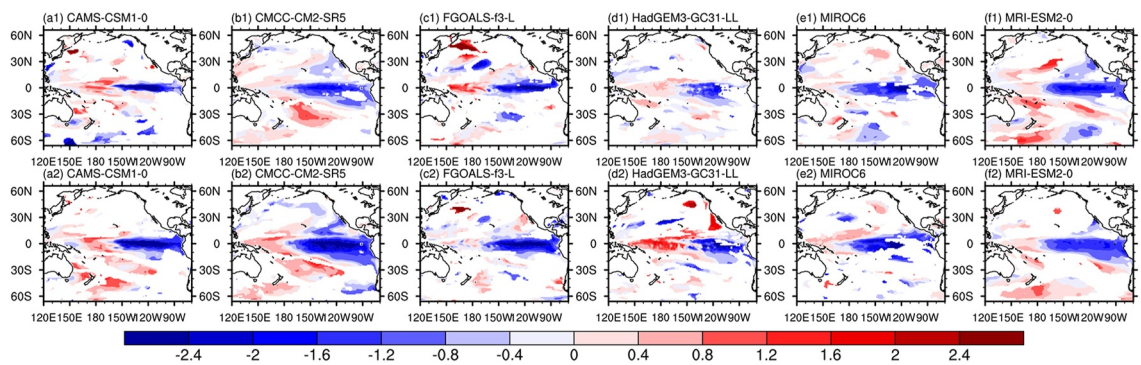

Figure 7. The composite difference (units: °C) between the two types of EP-Type errors and CP-Type errors in December for "Max Pred". (1) and (2) denote the difference between EP-Type-1 and CP-Type-1, and between EP-Type-2 and CP-Type-2, respectively. The shaded areas denote those exceeding the 90% significance level.

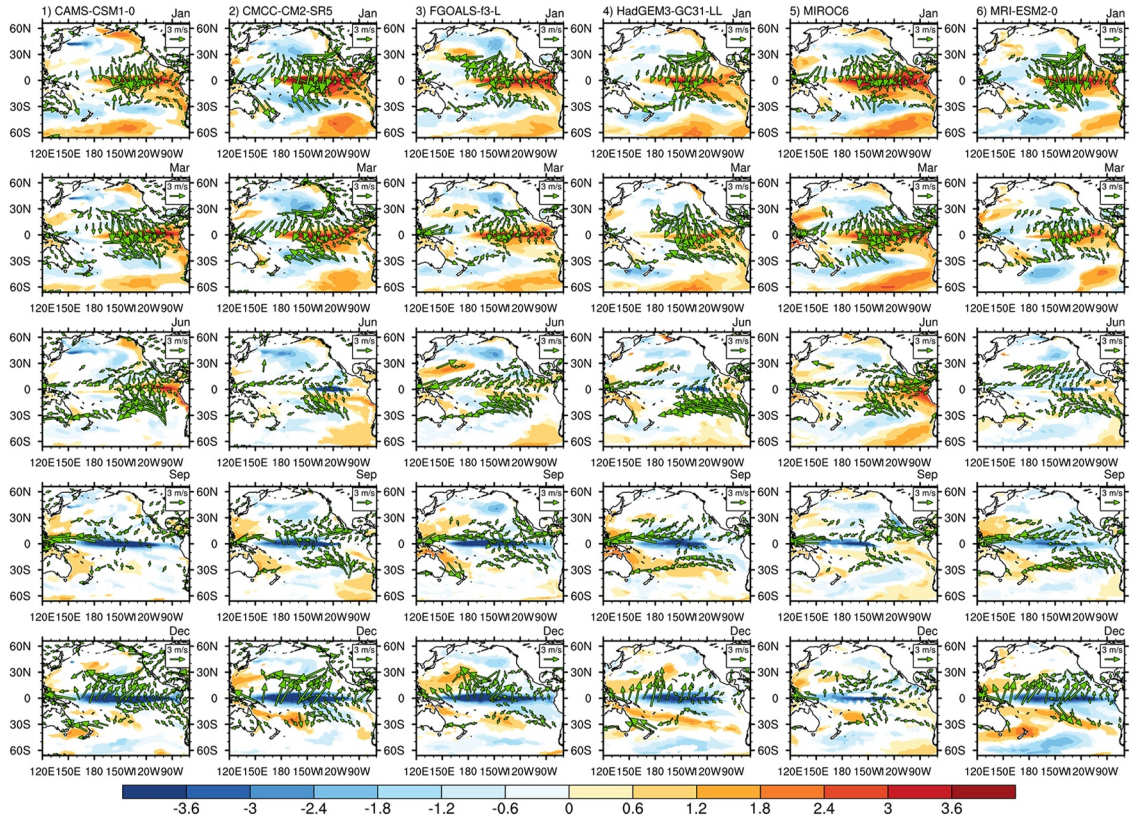

Figure 8. Composite evolutions of anomalous ocean temperature (shaded) (units: °C) and surface wind (vectors) (units: m/s) of CP-Type-1 errors for "Max PB", as shown in January, March, June, September, and December from top to bottom. The shaded areas denote those exceeding the 90% significance level. Only surface wind vectors significant at the 90% level are shown.

Furthermore, we also analyze the composite initial errors for "Max PB" (Figure 8 for CP-Type-1; Figure S19 in Supporting Information S1 for EP-Type-1; and others not shown). It is shown that the patterns and evolutions of two types of composite initial errors for "Max PB" are very similar to that for "Max Pred", and so, the overall amplitude difference is very small, regardless of CP or EP El Niño. The above conclusion confirms the inference in Section 3 that the initial errors between "Max Pred" and "Max PB" are very similar. Then, we further ask the following question: What is the difference between the specific initial errors for "Max Pred" and the SPB-related initial errors for "Often PB"? What is the indication of difference for the forecast of two types of El Nino events?

5. The Difference Between the Initial Errors That Cause the Largest Prediction Errors and the SPB-Related Initial Errors

To answer the above questions, we first analyze the SPB-related initial errors for "Often PB" (Figure 9). It is shown that CP-Type-1 (Figures 9a1–9e1) and EP-Type-1 (Figures 9a2–9e2) are very similar in spatial structures and evolutionary features. That is, the spatial structures of initial errors in the equatorial Pacific exhibit a dipole structure with positive errors in the upper central-eastern Pacific and negative errors in the lower western Pacific; in the South Pacific show the negative SPMM-like and in the North Pacific are the VM-like for most models. The evolutionary features of CP-Type-1 and EP-Type-1 start with the decay of El Niño-like, and then transition to the development of La Niña-like. Physically, the warm SSTA over the central-eastern equatorial Pacific promotes westward winds, and thus, evoked Kelvin waves in the ocean gradually transmit the cold SSTA in the lower region of western equatorial Pacific to be eastward and upward. Once the cold SST errors over the central-eastern equatorial Pacific appear and then gradually develop under the Bjerknes feedback. The negative SPMM-like cold SSTA and its induced southeasterly wind anomalies over the South Pacific promote the disappearance of warm SSTA and then contribute to the development of cold SSTA in the central-eastern equatorial Pacific through the WES feedback. However, the role of the VM-like SSTA mode over the North Pacific initial errors is opposite to

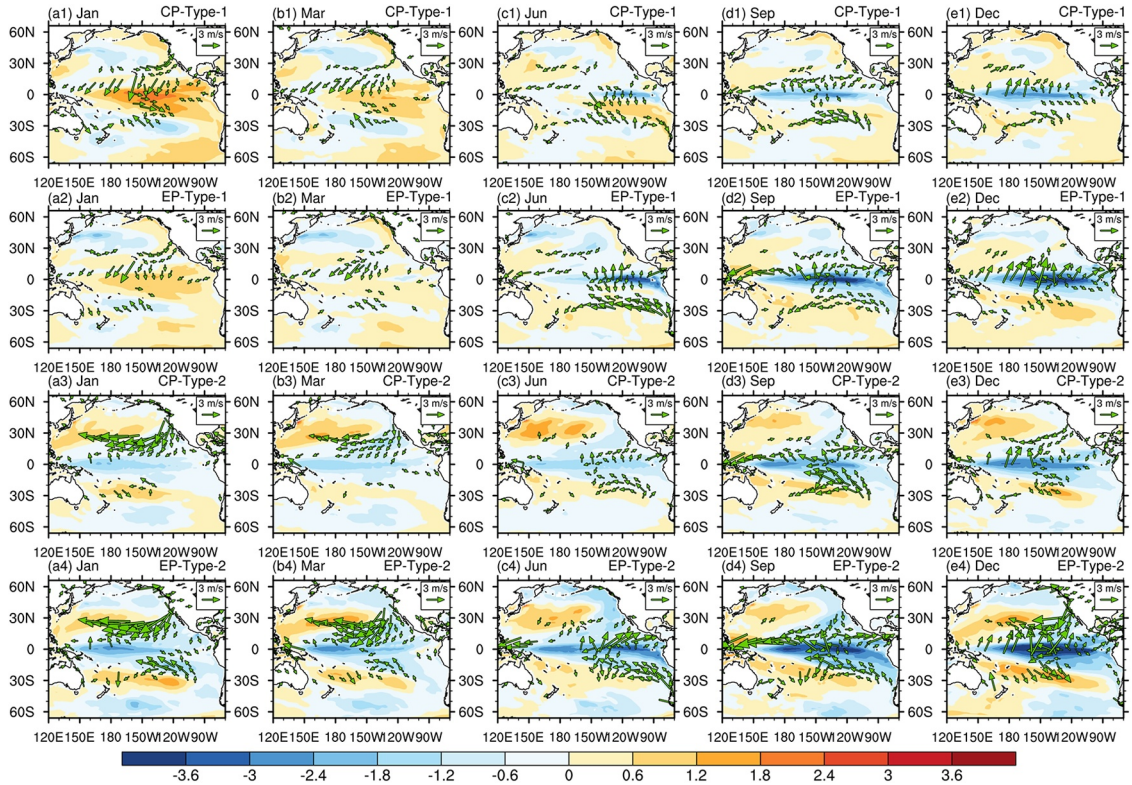

Figure 9. As in Figure 5, but for the two types of composite errors in CP and EP El Niño for "Often PB". This figure shows the results of the CMCC-CM2-SR5 model.

that of the two previous processes for the equatorial and South Pacific. Specifically, the warm SSTA near the Alaska Gulf induces the near-surface counterclockwise circulation anomalies through convective feedback, which tend to transport the warm SST to the equator (Hou et al., 2019).

Likewise, the spatial structures of SPB-related initial errors for CP-Type-2 (Figures 9a3–9e3) and EP-Type-2 (Figures 9a4–9e4) are very similar, showing opposite patterns compared to CP-Type-1 and EP-Type-1. The evolutionary characteristic of CP-Type-2 and EP-Type-2 show the development of La Niña-like in most models. However, the December cold SSTA of CP-Type-2 over the central equatorial Pacific is significantly weaker than that of EP-Type-2 over the central-eastern equatorial Pacific. Physically, the easterly wind anomalies accompanying the cold SST errors over the central-eastern equatorial Pacific are very weak in both CP-Type-2 and EP-Type-2, so the Bjerknes positive feedback is weak overall. The further comparison reveals that the negative VM-like SST errors over the North Pacific in EP-Type-2 contribute significantly stronger to the development of cold bias in the equatorial Pacific than that in CP-Type-2 during January–March. Thereafter, the contribution in the North Pacific of CP-Type-2 and EP-Type-2 diminishes for most models, and the role of South Pacific becomes prominent. The SPMM-like warm SSTA component on the western side of South Pacific always exists but does not induce significant northwesterly wind anomalies, regardless of the development process of CP-Type-2 or EP-Type-2. Over the southeastern Pacific near the equator, the cold SSTA and related southeasterly wind anomalies for EP-Type-2 are constantly developing and strengthening, especially from June to September. Nevertheless, the cold SSTA in the southeastern Pacific are always weak for CP-Type-2. In summary, the process of North and South Pacific in EP-Type-2 together leads to the stronger cold bias over the central-eastern equatorial Pacific. Whereas, the cold bias over the central equatorial Pacific caused by CP-Type-2 mainly benefits from the weaker contribution of North Pacific.

The composite difference between the CP-Type-1 errors evolution of "Max Pred" and that of "Often PB" is given in Figure 10 (Figure S20 in Supporting Information S1 for EP-Type-1). It is found that the difference is very similar to the evolutionary pattern of Type-1 errors for "Max Pred", regardless of CP El Niño or EP El Niño. Combined with the previous results, it is shown that the spatial patterns (in the equatorial and South Pacific) and evolution features of the Type-1 initial errors for "Max Pred" are very similar to that for "Often PB" in two types

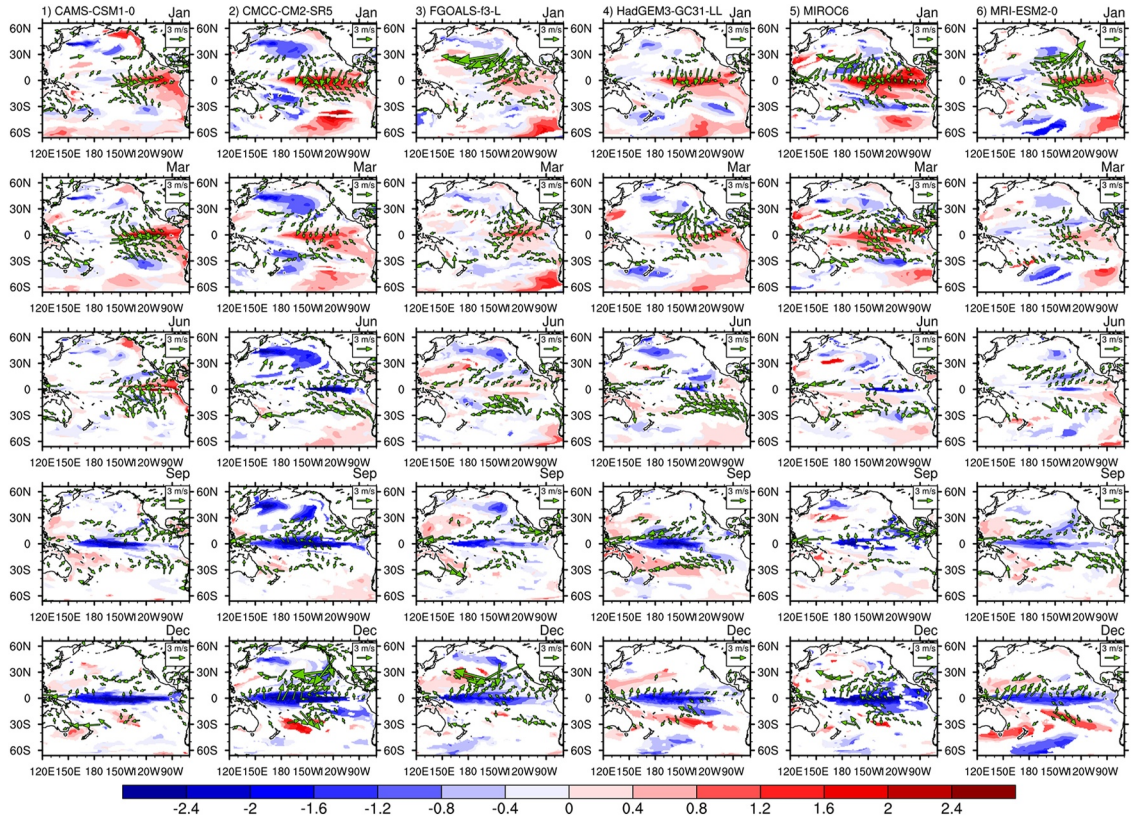

Figure 10. As in Figure 8, but for the composite difference (units: °C) between CP-Type-1 errors of "Max Pred" and CP-Type-1 errors of "Often PB".

of El Niño events, except that the amplitude is overall stronger than that of "Often PB". Whereas the spatial structures of Type-1 initial errors over the North Pacific for "Max Pred" show the negative VM-like SSTA mode, which is opposite to that of "Often PB". Furthermore, the biggest difference of initial errors between "Max Pred" and "Often PB" is reflected in the Type-2 initial errors for two types of El Nino events. In terms of spatial structures, the patterns are almost opposite in the equatorial Pacific and South Pacific, and similar in the North Pacific with the negative VM-like SSTA mode (Figures S16 and S18 in Supporting Information S1 vs. Figure 9). Correspondingly, the evolution features are different in the early stage, but both of them eventually show the development of La Niña-like. However, although the initial errors of Type-2 for "Max Pred" show the warm SSTA over the equatorial Pacific, the cold SST errors is still significantly stronger than that of "Often PB" at the final time (not shown). In summary, it indicates that despite the two types of composite initial errors for "Max Pred" have larger warm SSTAs in the equatorial Pacific, such initial errors identified in the present study have stronger positive feedback processes acting together in the equatorial Pacific, North and South Pacific, which can have more serious impacts on the final prediction of two types of El Niño events.

6. Summary and Discussion

The existence of the season-dependent PB phenomenon and the frequent occurrence of CP El Niño are two of the main reasons affecting the ENSO prediction skills since 2000. Therefore, many efforts have been made to explore the predictability dynamics of the two types of El Niño events associated with the initial uncertainties in ocean temperature from the perspective of season-dependent PB (e.g., Hou et al., 2019; Qi et al., 2021). However, few studies investigate the relationship between forecasts and initial errors (and with the corresponding PB) by directly considering the largest prediction errors. Duan et al. (2024) proposed the new method, namely, the coupled conditional nonlinear optimal perturbation (C-CNOP) method, which expects to adequately capture the nonlinear unstable growth of initial uncertainties, and also be able to take into account the effect of the coupling processes uncertainty on initial perturbations. Therefore, based on the C-CNOP method, this study

explores the predictability dynamics of two types of El Niño events from the perspective of initial errors growth by using the pi-Control outputs of CMIP6 coupled models.

In contrast to the forecast series related to season-dependent PB (denoted as "Often PB"), which are commonly analyzed in previous studies, this study adds two types of forecast series targeting different optimization problems (i.e., "Max Pred" with the greatest influence on the prediction and "Max PB" with the strongest PB). The results show that CP El Niño forecasts tend to experience the summer PB, while EP El Niño forecasts often occur the spring PB for three types of forecast series. The intensity of seasonal-dependent PB and the magnitude of prediction errors between "Max Pred" and "Max PB" are very similar, indicating that only powerful season-dependent PB can lead to large prediction errors.

Specific initial errors are the necessary condition to generate the seasonal-dependent PB. Then, we first focus on analyzing the spatial structures, evolutionary characteristics, and evolutionary mechanisms of the initial errors for "Max Pred". For CP El Niño, the spatial patterns of CP-Type-1 and CP-Type-2 errors are very similar. That is, the equatorial Pacific exhibits the SSTA dipole structure of east positive–west negative, the upper layers of North Pacific are similar to the negative VM mode, and the upper layers of South Pacific show a general resemblance to the negative SPMM mode. Differently, the magnitude of CP-Type-2 initial errors is overall smaller than that of CP-Type-1. The evolutions of two types of errors start with the decay of El Niño-like mode, and then transition to the development of La Niña-like mode. Physically, the positive feedback processes in the equatorial Pacific, North and South Pacific ultimately combine to result in large negative errors over the central-eastern equatorial Pacific in December, causing underestimations of the intensity of CP El Niño events and perhaps even influencing its structure. For EP El Niño, the spatial patterns and evolutions of EP-Type-1 and EP-Type-2 errors are similar to that of CP-Type-1 and CP-Type-2, but ultimately triggering more easterly regions of the equatorial cold bias in December. Further analysis reveals that the SSTA mode of negative VM-like for CP El Niño plays a stronger role than that for EP El Niño, whereas the negative SPMM-like SSTA mode for EP El Niño plays a stronger role than that for CP El Niño. Therefore, the two types of El Niño events with similar errors are made to have different locations of the equatorial cold bias. Moreover, the patterns and evolutions of two types of composite initial errors for "Max PB" are very similar to that for "Max Pred", regardless of CP or EP El Niño.

Finally, we pay further attention to delving into the difference between the specific initial errors for "Max Pred" and the SPB-related initial errors for "Often PB". The spatial patterns (in the equatorial and South Pacific) and evolution features of CP-Type-1 and EP-Type-1 for "Max Pred" are very similar to that for "Often PB". Whereas the spatial structures of Type-1 initial errors over the North Pacific for "Max Pred" is opposite to that of "Often PB". Furthermore, the spatial patterns of CP-Type-2 and EP-Type-2 between "Max Pred" and "Often PB" are almost opposite in the equatorial Pacific and South Pacific, and similar in the North Pacific. Consequently, the evolution features are different in the early stage, but both of them eventually show the development of La Niña-like. Anyway, the initial errors of "Max Pred" and "Max PB" identified in the present study can have more serious impacts on the final prediction of two types of El Niño events.

The adaptive observation technique that can help to design the observation strategy with a limited number of observations in some critical areas is expected to improve prediction skills for high-impact weather or climate events at the lowest cost (Jiang et al., 2024; Mu et al., 2015). Therefore, if we deploy observations by using the adaptive observation in some critical areas of the equatorial Pacific, North and South Pacific, where the initial errors of "Max Pred" or "Max PB" are large and concentrated, it will be possible to maximize prediction skills for two types of El Niño events. The key point is that improvements to the accuracy of initial SST in the North and South Pacific may even be very helpful in distinguishing the type of El Niño. Further comparison reveals that the evolution of El Niño and its error growth have a similar mechanism, and thus, these observations are also helpful in identifying the precursor perturbations of El Niño. Additionally, Hou et al. (2019) using the CMIP5 coupled model, show that EP El Niño is less predictable than CP El Niño. This study also found that the season-dependent PB of EP El Niño occurs earlier than that of CP El Niño, and the PB of EP El Niño is stronger, which may further indicate that successful prediction for EP El Niño is more difficult than that for CP El Niño. However, the actual forecast models still have large biases for the prediction of CP-El Niño events, which may be one of the main reasons for the higher actual prediction skills of EP El Niño than CP-El Niño (Fang & Chen, 2023; Zheng & Yu, 2017). Also, it seems that there is no qualitative improvement in the simulations of CP El Niño from CMIP5 to CMIP6, so model development remains one of the priorities on ENSO research (Hou & Tang, 2022). In the future, with the continuous development of models, it is worthy to further explore how the heterogeneous

predictability (i.e., the actual prediction skills; Kumar et al., 2016; Jin, 2022) of the two types of El Niño events will change. Another interesting topic is how long can the effects of the coupled initial perturbations of this study on the forecast results continue in the actual forecast models, considering model errors? It is thereby worth to further examine the ENSO predictability dynamics by using the more advanced method in references (e.g., Andreou & Chen, 2024; Fang & Chen, 2023). Lastly, as stated in Section 2, we realize that the irregularity of ENSO is the result of multiscale interactions. Therefore, the present study describes the coupled perturbations by using the deterministic equations of the C-CNOP method, which can handle different scale processes (e.g., ocean and atmosphere). However, the C-CNOP method is not yet able to deal with the effects of stochastic processes on ENSO as proposed in some recent papers (Chen et al., 2022; Geng et al., 2020), and this issue is worth exploring in-depth in the future.

Data Availability Statement

The monthly CMIP6 data sets are available at https://esgf-node.llnl.gov/projects/cmip6/.

Acknowledgments
This study was supported by the National Natural Science Foundation of China (42330111, 42375063) and Key Natural Science Foundation of Gansu Province (23JRRA1030).

References

Andreou, M., & Chen, N. (2024). Statistical response of ENSO complexity to initial condition and model parameter perturbations. *Journal of Climate*, *37*(21), 5629–5651. (published online ahead of print 2024). https://doi.org/10.1175/JCLI-D-24-0017.1

Barnston, A. G., Tippett, M. K., L'Heureux, M. L., Li, S., & DeWitt, D. G. (2012). Skill of real-time seasonal ENSO model predictions during 2002–11: Is our capability increasing? *Bulletin of the American Meteorological Society*, *93*(5), 631–651. https://doi.org/10.1175/bams-d-11-00111.1

Bellenger, H., Guilyardi, E., Leloup, J., Lengaigne, M., & Vialard, J. (2014). ENSO representation in climate models: From CMIP3 to CMIP5. *Climate Dynamics*, *42*(7–8), 1999–2018. https://doi.org/10.1007/S00382-013-1783-Z

Bjerknes, J. (1969). Atmospheric teleconnections from the equatorial Pacific. *Monthly Weather Review*, *97*(3), 163–172. https://doi.org/10.1175/1520-0493(1969)097<0163:ATFTEP>2.3.CO;2

Chen, D., Cane, M. A., Kaplan, A., Zebiak, S. E., & Huang, D. (2004). Predictability of El Niño over the past 148 years. *Nature*, *428*(6984), 733–736. https://doi.org/10.1038/nature02439

Chen, D., Zebiak, S. E., Busalacchi, A. J., & Cane, M. A. (1995). An improved procedure for El Niño forecasting: Implications for predictability. *Science*, *269*(5231), 1699–1702. https://doi.org/10.1126/science.269.5231.1699

Chen, M., Yu, J. Y., Wang, X., & Jiang, W. (2019). The changing impact mechanisms of a diverse El Niño on the Western Pacific subtropical high. *Geophysical Research Letters*, *46*(2), 953–962. https://doi.org/10.1029/2018gl081131

Chen, N., Fang, X. H., & Yu, J. Y. (2022). A multiscale model for El Niño complexity. *npj Climate and Atmospheric Science*, *5*(1), 16. https://doi.org/10.1038/s41612-022-00241-x

Ding, R. Q., Li, J. P., & Tseng, Y. H. (2015). The impact of South Pacific extratropical forcing on ENSO and comparisons with the North Pacific. *Climate Dynamics*, *44*(7–8), 2017–2034. https://doi.org/10.1007/s00382-014-2303-5

Duan, W. S., & Hu, J. Y. (2016). The initial errors that induce a significant "spring predictability barrier" for El Niño events and their implications for target observation: Results from an earth system model. *Climate Dynamics*, *46*(11–12), 3599–3615. https://doi.org/10.1007/s00382-015-2789-5

Duan, W. S., Hu, L., & Feng, R. (2024). Coupled conditional nonlinear optimal perturbations and their application to ENSO ensemble forecasts. *Science China Earth Sciences*, *67*(3), 826–842. https://doi.org/10.1007/s11430-023-1273-1

Duan, W. S., Liu, X. C., Zhu, K. Y., & Mu, M. (2009). Exploring the initial errors that cause a significant "spring predictability barrier" for El Niño events. *Journal of Geophysical Research*, *114*(C4), C04022. https://doi.org/10.1029/2008jc004925

Duan, W. S., & Wei, C. (2013). The "spring predictability barrier" for ENSO predictions and its possible mechanism: Results from a fully coupled model. *International Journal of Climatology*, *33*(5), 1280–1292. https://doi.org/10.1002/joc.3513

Eyring, V., Bony, S., Meehl, G. A., Senior, C. A., Stevens, B., Stouffer, R. J., & Taylor, K. E. (2016). Overview of the Coupled Model Intercomparison Project Phase 6 (CMIP6) experimental design and organization. *Geoscientific Model Development*, *9*(5), 1937–1958. https://doi.org/10.5194/gmd-9-1937-2016

Fang, X., & Chen, N. (2023). Quantifying the predictability of ENSO complexity using a statistically accurate multiscale stochastic model and information theory. *Journal of Climate*, *36*(8), 2681–2702. https://doi.org/10.1175/JCLI-D-22-0151.1

Food and Agriculture Organization of the United Nations. (2016). El Niño and La Niña: Preparedness and response, situation report July 2016. Retrieved from http://www.fao.org/fileadmin/user_upload/emergencies/docs/FAOElNinoSitRep_versionJULY.pdf

Geng, T., Cai, W., & Wu, L. (2020). Two types of ENSO varying in tandem facilitated by nonlinear atmospheric convection. *Geophysical Research Letters*, *47*(15), e2020GL088784. https://doi.org/10.1029/2020GL088784

Hong, L. C., & Jin, F. F. (2014). A southern hemisphere booster of super El Niño. *Geophysical Research Letters*, *41*(6), 2142–2149. https://doi.org/10.1002/2014GL059370

Hou, M. Y., Duan, W. S., & Zhi, X. F. (2019). Season-dependent predictability barrier for two types of El Niño revealed by an approach to data analysis for predictability. *Climate Dynamics*, *53*(9–10), 5561–5581. https://doi.org/10.1007/s00382-019-04888-w

Hou, M. Y., & Tang, Y. M. (2022). Recent progress in simulating two types of ENSO–from CMIP5 to CMIP6. *Frontiers in Marine Science*, *9*, 986780. https://doi.org/10.3389/fmars.2022.986780

Hou, Z., Li, J., Ding, R., & Feng, J. (2022). Investigating decadal variations of the seasonal predictability limit of sea surface temperature in the tropical Pacific. *Climate Dynamics*, *59*(3–4), 1079–1096. https://doi.org/10.1007/s00382-022-06179-3

Jiang, L., Duan, W., & Wang, H. (2024). The sensitive area for targeting observations of paired mesoscale eddies associated with sea surface height anomaly forecasts. *Journal of Geophysical Research: Oceans*, *129*(2), e2023JC020572. https://doi.org/10.1029/2023JC020572

Jin, Y. S. (2022). The signal-to-noise paradox in ENSO prediction: Role of ENSO growth rate and period. *Geophysical Research Letters*, *49*(12), e2022GL097965. https://doi.org/10.1029/2022GL097965

Jin, Y. S., Liu, Z. Y., Lu, Z. Y., & He, C. F. (2019). Seasonal cycle of background in the tropical Pacific as a cause of ENSO spring persistence barrier. *Geophysical Research Letters*, *46*(22), 13371–13378. https://doi.org/10.1029/2019GL085205

Kug, J. S., Jin, F. F., & An, S. I. (2009). Two types of El Niño events: Cold tongue El Niño and warm pool El Niño. *Journal of Climate*, *22*(6), 1499–1515. https://doi.org/10.1175/2008jcli2624.1

Kumar, A., Hu, Z. Z., Jha, B., & Peng, P. T. (2016). Estimating ENSO predictability based on multi-model hindcasts. *Climate Dynamics*, *48*(1–2), 39–51. https://doi.org/10.1007/s00382-016-3060-4

Latif, M., Anderson, D., Barnett, T., Cane, M., Kleeman, R., Leetmaa, A., et al. (1998). A review of the predictability and prediction of ENSO. *Journal of Geophysical Research*, *103*(C7), 14375–14393. https://doi.org/10.1029/97JC03413

Lau, K. M., & Yang, S. (1996). The Asian monsoon and predictability of the tropical ocean-atmosphere system. *Quarterly Journal of the Royal Meteorological Society*, *122*(532), 945–957. https://doi.org/10.1256/smsqj.53207

Lee, H. C., Kumar, A., & Wang, W. Q. (2018). Effects of ocean initial perturbation on developing phase of ENSO in a coupled seasonal prediction model. *Climate Dynamics*, *50*(5–6), 1747–1767. https://doi.org/10.1007/s00382-017-3719-5

Levine, A. F. Z., & McPhaden, M. J. (2015). The annual cycle in ENSO growth rate as a cause of the spring predictability barrier. *Geophysical Research Letters*, *42*(12), 5034–5041. https://doi.org/10.1002/2015gl064309

Liu, Z. Y., Jin, Y. S., & Rong, X. Y. (2019). A theory for the seasonal predictability barrier: Threshold, timing, and intensity. *Journal of Climate*, *32*(2), 423–443. https://doi.org/10.1175/jcli-d-18-0383.1

Lorenz, E. N. (1975). Climatic predictability in the physical basis of climate and climate modeling. *WMO GARP Publ. Ser No*, *16*, 132–136.

McPhaden, M. J. (1999). Genesis and evolution of the 1997-98 El Niño. *Science*, *283*(5404), 950–954. https://doi.org/10.1126/science.283.5404.950

McPhaden, M. J. (2003). Tropical Pacific Ocean heat content variations and ENSO persistence barriers. *Geophysical Research Letters*, *30*(9), 1480. https://doi.org/10.1029/2003gl016872

McPhaden, M. J., Zebiak, S. E., & Glantz, M. H. (2006). ENSO as an integrating concept in earth science. *Science*, *314*(5806), 1740–1745. https://doi.org/10.1126/science.1132588

Min, Q. Y., Su, J. Z., & Zhang, R. H. (2017). Impact of the South and North Pacific meridional modes on the El Niño–southern oscillation: Observational analysis and comparison. *Journal of Climate*, *30*(5), 1705–1720. https://doi.org/10.1175/JCLI-D-16-0063.1

Min, Q. Y., Su, J. Z., Zhang, R. H., & Rong, X. Y. (2015). What hindered the El Niño pattern in 2014? *Geophysical Research Letters*, *42*(16), 6762–6770. https://doi.org/10.1002/2015GL064899

Mu, M., Duan, W. S., Chen, D. K., & Yu, W. D. (2015). Target observations for improving initialization of high-impact ocean-atmospheric environmental events forecasting. *National Science Review*, *2*, 226–236. https://doi.org/10.1093/nsr/nwv021

Mu, M., Duan, W. S., & Tang, Y. M. (2017). The predictability of atmospheric and oceanic motions: Retrospect and prospects. *Science China Earth Sciences*, *60*(11), 2001–2012. https://doi.org/10.1007/s11430-016-9101-x

Mu, M., Xu, H., & Duan, W. S. (2007). A kind of initial errors related to "spring predictability barrier" for El Niño events in Zebiak-Cane model. *Geophysical Research Letters*, *34*(3), L03709. https://doi.org/10.1029/2006gl027412

Philander, S. G. H. (1983). El-niño southern oscillation phenomena. *Nature*, *302*(5906), 295–301. https://doi.org/10.1038/302295a0

Planton, Y. Y., Guilyardi, E., Wittenberg, A. T., Lee, J., Gleckler, P. J., Bayr, T., et al. (2021). Evaluating climate models with the CLIVAR 2020 ENSO metrics package. *Bulletin of the American Meteorological Society*, *102*(2), E193–E217. https://doi.org/10.1175/BAMS-D-19-0337.1

Qi, Q. Q., Duan, W. S., & Xu, H. (2021). The most sensitive initial error modes modulating intensities of CP- and EP-El Niño events. *Dynamics of Atmospheres and Oceans*, *96*, 101257. https://doi.org/10.1016/j.dynatmoce.2021.101257

Ren, H. L., & Jin, F. F. (2011). Niño indices for two types of ENSO. *Geophysical Research Letters*, *38*(4), L04704. https://doi.org/10.1029/2010GL046031

Ren, H. L., Zuo, J. Q., & Deng, Y. (2018). Statistical predictability of Niño indices for two types of ENSO. *Climate Dynamics*, *52*(9–10), 5361–5382. https://doi.org/10.1007/s00382-018-4453-3

Samelson, R. M., & Tziperman, E. (2001). Instability of the chaotic ENSO: The growth-phase predictability barrier. *Journal of the Atmospheric Sciences*, *58*(23), 3613–3625. https://doi.org/10.1175/1520-0469(2001)058<3613:IOTCET>2.0.CO;2

Sánchez-Murillo, R., Durán-Quesada, A. M., Birkel, C., Esquivel-Hernández, G., & Boll, J. (2017). Tropical precipitation anomalies and d-excess evolution during El Niño 2014-16. *Hydrological Processes*, *31*(4), 956–967. https://doi.org/10.1002/hyp.11088

Schulzweida, U. (2022). *CDO user guide* (Vol. 10). Zenodo. https://doi.org/10.5281/zenodo.7112925

Su, J. Z., Xiang, B. Q., Wang, B., & Li, T. (2014). Abrupt termination of the 2012 Pacific warming and its implication on ENSO prediction. *Geophysical Research Letters*, *41*(24), 9058–9064. https://doi.org/10.1002/2014gl062380

Tang, Y. M., Zhang, R. H., Liu, T., Duan, W., Yang, D., Zheng, F., et al. (2018). Progress in ENSO prediction and predictability study. *National Science Review*, *5*(6), 826–839. https://doi.org/10.1093/nsr/nwy105

Tao, L., Mu, M., Wang, L., Fang, X., Duan, W., & Zhang, R. H. (2023). Impacts of initial zonal current errors on the predictions of two types of El Niño events. *Journal of Geophysical Research: Oceans*, *128*(6), e2023JC019833. https://doi.org/10.1029/2023JC019833

Thompson, C. J., & Battisti, D. S. (2001). A linear stochastic dynamical model of ENSO. Part II: Analysis. *Journal of Climate*, *14*(4), 445–466. https://doi.org/10.1175/1520-0442(2001)014<0445:ALSDMO>2.0.CO;2

Tian, B., & Duan, W. S. (2016). Comparison of the initial errors most likely to cause a spring predictability barrier for two types of El Niño events. *Climate Dynamics*, *47*(3–4), 779–792. https://doi.org/10.1007/s00382-015-2870-0

Timmermann, A., An, S. I., Kug, J. S., Jin, F. F., Cai, W., Capotondi, A., et al. (2018). El Niño-southern oscillation complexity. *Nature*, *559*(7715), 535–545. https://doi.org/10.1038/s41586-018-0252-6

Torrence, C., & Webster, P. J. (1998). The annual cycle of persistence in the El Niño southern oscillation. *The Quarterly Journal of the Royal Meteorological Society*, *124*(550), 1985–2004. https://doi.org/10.1002/qj.49712455010

Valle, C. A., Cruz, F., Cruz, J. B., Merlen, G., & Coulter, M. C. (1987). The impact of the 1982–1983 E1 Niño-southern oscillation on seabirds in the Galapagos Islands, Ecuador. *Journal of Geophysical Research*, *92*(C13), 14437–14444. https://doi.org/10.1029/JC092iC13p14437

Vimont, D. J., Wallace, J. M., & Battisti, D. S. (2003). The seasonal footprinting mechanism in the Pacific: Implications for ENSO. *Journal of Climate*, *16*(16), 2668–2675. https://doi.org/10.1175/1520-0442(2003)016<2668:tsfmit>2.0.co;2

Wang, R., & Ren, H. L. (2017). The linkage between two ENSO types/modes and the interdecadal changes of ENSO around the year 2000. *Atmospheric and Oceanic Science Letters*, *10*(2), 168–174. https://doi.org/10.1080/16742834.2016.1258952

Wang, X., Guan, C., Huang, R. X., Tan, W., & Wang, L. (2019). The roles of tropical and subtropical wind stress anomalies in the El Niño Modoki onset. *Climate Dynamics*, *52*(11), 6585–6597. https://doi.org/10.1007/s00382-018-4534-3

Webster, P. J. (1995). The annual cycle and the predictability of the tropical coupled ocean-atmosphere system. *Meteorology and Atmospheric Physics*, *56*(1–2), 33–55. https://doi.org/10.1007/bf01022520

Webster, P. J., & Yang, S. (1992). Monsoon and ENSO: Selectively interactive systems. *Quarterly Journal of the Royal Meteorological Society*, *118*(507), 877–926. https://doi.org/10.1256/smsqj.50704

Xie, S. P., & Philander, G. (1994). A coupled ocean-atmosphere model of relevance to the ITCZ in the eastern Pacific. *Tellus, Series A*, *46 A*(4), 340–350. https://doi.org/10.3402/tellusa.v46i4.15484

Xue, Y., Cane, M. A., Zebiak, S. E., & Blumenthal, M. B. (1994). On the prediction of ENSO: A study with a low-order Markov model. *Tellus*, *46*(4), 512–528. https://doi.org/10.1034/j.1600-0870.1994.00013.x

Yeh, S. W., Kug, J. S., & An, S. I. (2014). Recent progress on two types of El Niño: Observations, dynamics, and future changes. *Asia-Pacific Journal of Atmospheric Sciences*, *50*(1), 69–81. https://doi.org/10.1007/s13143-014-0028-3

Yeh, S. W., Kug, J. S., Dewitte, B., Kwon, M. H., Kirtman, B. P., & Jin, F. F. (2009). El Niño in a changing climate. *Nature*, *461*(7263), 511–514. https://doi.org/10.1038/nature08316

Yeh, S. W., Wang, X., Wang, C., & Dewitte, B. (2015). On the relationship between the North Pacific climate variability and the central Pacific El Niño. *Journal of Climate*, *28*(2), 663–677. https://doi.org/10.1175/jcli-d-14-00137.1

Yu, J. Y., & Kim, S. T. (2011). Relationships between extratropical sea level pressure variations and the central Pacific and eastern Pacific types of ENSO. *Journal of Climate*, *24*(3), 708–720. https://doi.org/10.1175/2010jcli3688.1

Yu, Y. S., Duan, W. S., Xu, H., & Mu, M. (2009). Dynamics of nonlinear error growth and season-dependent predictability of El Niño events in the Zebiak-Cane model. *The Quarterly Journal of the Royal Meteorological Society*, *135*(645), 2146–2160. https://doi.org/10.1002/qj.526

Zhai, P., Yu, R., Guo, Y., Li, Q., Ren, X., Wang, Y., et al. (2016). The strong El Niño of 2015/16 and its dominant impacts on global and China's climate. *Journal of Meteorological Research*, *30*(3), 283–297. https://doi.org/10.1007/s13351-016-6101-3

Zhang, H., Clement, A., & Di Nezio, P. (2014). The South Pacific meridional mode: A mechanism for ENSO-like variability. *Journal of Climate*, *27*(2), 769–783. https://doi.org/10.1175/jcli-d-13-00082.1

Zhang, J., Duan, W. S., & Zhi, X. F. (2015). Using CMIP5 model outputs to investigate the initial errors that cause the "spring predictability barrier" for El Niño events. *Science China Earth Sciences*, *58*(5), 685–696. https://doi.org/10.1007/s11430-014-4994-1

Zhang, W., Jin, F. F., Stuecker, M. F., Wittenberg, A. T., Timmermann, A., Ren, H. L., et al. (2016). Unraveling El Niño's impact on the east Asian monsoon and Yangtze river summer flooding. *Geophysical Research Letters*, *43*(21), 11375–11382. https://doi.org/10.1002/2016GL071190

Zheng, F., Fang, X. H., Yu, J. Y., & Zhu, J. (2014). Asymmetry of the Bjerknes positive feedback between the two types of El Niño. *Geophysical Research Letters*, *41*(21), 7651–7657. https://doi.org/10.1002/2014GL062125

Zheng, F., & Yu, J. Y. (2017). Contrasting the skills and biases of deterministic predictions for the two types of El Niño. *Advances in Atmospheric Sciences*, *34*(12), 1395–1403. https://doi.org/10.1007/s00376-017-6324-y